ACADEMIC PRESS

Available online at www.sciencedirect.com
SCIENCE DIRECT®

Journal of Catalysis 219 (2003) 85–96

JOURNAL OF CATALYSIS

www.elsevier.com/locate/jcat

Synthesis and characterization of silica-supported transition-metal phosphides as HDN catalysts

V. Zuzaniuk and R. Prins *

Institute for Chemical and Bioengineering, Swiss Federal Institute of Technology, ETH Hönggerberg, 8093 Zürich, Switzerland

Received 8 October 2002; revised 28 March 2003; accepted 28 March 2003

Abstract

Supported transition-metal phosphides (Co_2P/SiO_2, MoP/SiO_2, WP/SiO_2, $CoMoP/SiO_2$, and $NiMoP/SiO_2$) were prepared by means of pore-volume impregnation of a silica support. The metal oxide/phosphate precursors were reduced either in pure H_2 or in a flow of 4.8% H_2 in Ar. The materials obtained were characterized by CO chemisorption, powder X-ray diffractometry, and ^{31}P MAS NMR spectroscopy. The catalysts were tested in the hydrodenitrogenation of *o*-methylaniline at 643 K and 3 MPa in the presence and absence of H_2S. All the materials were active in this reaction, MoP/SiO_2 displaying the highest catalytic activity. In the presence of H_2S, all the catalysts lost some activity.

Keywords: Transition-metal phosphides; Temperature-programmed reduction; MAS NMR spectroscopy; Knight shift; Hydrodenitrogenation; *o*-Methylaniline

1. Introduction

Standard hydrodenitrogenation/hydrodesulfurization (HDN/HDS) catalysts consist of MoS_2-type phases supported on γ-Al_2O_3 and promoted by Co or Ni [1–3]. More stringent environmental regulations will mean that the activity of such materials must be improved. Thus, there is growing interest in developing alternatives to the widely used sulfides, which include transition-metal carbides, nitrides, and phosphides [4–15]. Transition-metal phosphide catalysts have been studied in hydrogenation reactions for some time [16–19] but research focused on their hydrotreating activities only recently [8–15]. The observation that the addition of phosphorus, as phosphate, had a promotional effect on the HDN activity of commercial sulfided Ni(or Co)–Mo/Al_2O_3 led to a growing interest in transition-metal phosphides as hydrotreating catalysts [8,20–22]. One explanation for the positive effect of phosphorus may be that phosphide-like species form under the reductive HDN conditions.

Co_2P and Ni_2P were prepared by the reduction of their respective metal phosphate and were active in the HDN of quinoline [8]. Bulk MoP was also synthesized by reducing an amorphous molybdenum phosphate and was catalytically active in the HDN of quinoline [9] and *o*-propylaniline [10]. In this research, MoP was found to be more active than an Al_2O_3-supported MoS_2 catalyst. Different binary and ternary transition-metal phosphides, Co_2P, Ni_2P, WP, MoP, NiMoP, CoMoP, and MoP, were also successfully prepared by H_2 reduction of a metal oxide/phosphate mixture and were tested in the HDN of *o*-propylaniline [11]. All the materials displayed an HDN activity, MoP being the most active. In the presence of H_2S, all the phosphides but WP lost activity. Bulk WP [12] and SiO_2-supported WP [13] were tested in the simultaneous removal of N and S from a simulated light oil fraction and their activity was compared to that of WC, W_2N, and WS_2. The unsupported phosphide material displayed the best performance in both the HDN of quinoline and the HDS of dibenzothiophene. In order to obtain a high dispersion, transition-metal phosphides were supported on carriers such as γ-Al_2O_3 or SiO_2 [13–15]. Silica-supported nickel phosphides with different Ni-to-P ratios, e.g., Ni_2P/SiO_2, $Ni_{12}P_5/SiO_2$, and Ni_3P/SiO_2, were prepared by reducing nickel oxide/phosphate precursors with H_2 [14]. This study showed that it is more difficult to synthesize supported transition-metal phosphides than unsupported samples. To obtain the desired stoichiometry, an

* Corresponding author.
E-mail address: prins@tech.chem.ethz.ch (R. Prins).

0021-9517/$ – see front matter
doi:10.1016/S0021-9517(03)00149-0

excess of phosphorus was added to the SiO_2 support. In other words, a Ni-to-P ratio of 2 to 1.3 was necessary to synthesize Ni_2P/SiO_2. A smaller amount of phosphorus resulted in the formation of phosphides such as $Ni_{12}P_5/SiO_2$ and Ni_3P/SiO_2. Using γ-Al_2O_3 as a support leads to even stronger interactions between the alumina and the phosphate precursors, which can react to form aluminum phosphate. Oyama et al. reported the preparation of alumina-supported molybdenum phosphide [15]. However, high loadings of molybdenum and phosphorus on the low surface area Al_2O_3 (91 $m^2\,g^{-1}$) were necessary to detect MoP phases by X-ray diffraction. This MoP/Al_2O_3 catalyst was tested in the simultaneous HDN of quinoline and the HDS of dibenzothiophene and performed better than a sulfided commercial $Ni–Mo–S/Al_2O_3$.

Our research focused on the preparation of binary and ternary transition-metal phosphides supported on SiO_2 (Co_2P/SiO_2, MoP/SiO_2, WP/SiO_2, $CoMoP/SiO_2$, and $NiMoP/SiO_2$). These phosphidic materials were prepared by reducing in H_2 a preimpregnated metal oxide/phosphate precursor on a silica support. The activity of those catalysts was compared to a classical $Ni–MoS_2/Al_2O_3$ catalyst with regard to the HDN of *o*-methylaniline (OMA) at 643 K and 3.0 MPa.

2. Experimental

2.1. Catalyst preparation

Supported phosphides (Co_2P, MoP, WP, CoMoP, and NiMoP) were prepared by pore-volume impregnation of a silica support. The silica support (chromatography gel, C-560, CU Chemie Uetikon, surface area 500 $m^2\,g^{-1}$, pore volume after drying 1 $ml\,g^{-1}$) was ground, sieved (63–90 μm), and dried for 12 h at 393 K. Di-ammonium hydrogen phosphate $(NH_4)_2HPO_4$ was the phosphorus source. Table 1 lists the different metal salt precursors used during the synthesis, together with the metal loadings and P-to-metal ratios. To avoid the formation of an insoluble precipitate of cobalt phosphate upon mixing aqueous solutions of cobalt nitrate ($Co(NO_3)_2 \cdot 6H_2O$) and ammonium phosphate ($(NH_4)_2HPO_4$), a two-step impregnation was performed to prepare the supported cobalt phosphide. The metal solution was introduced onto the SiO_2 surface, which was then dried at 393 K. $(NH_4)_2HPO_4$ solution was added to the support, and the resulting material was dried at 393 K and calcined at 623 K. In the case of MoP/SiO_2 and WP/SiO_2, the metal salt solution ($(NH_4)_6Mo_7O_{24} \cdot 4H_2O$ and $(NH_4)_6H_2W_{12}O_{40} \cdot 18H_2O$, respectively) was added to the phosphate solution prior to the impregnation on the support. The precursors of the ternary phosphides ($CoMoP/SiO_2$ and $NiMoP/SiO_2$) were prepared in two impregnation steps: a mixed solution of $(NH_4)_2HPO_4$ and $(NH_4)_6Mo_7O_{24} \cdot 4H_2O$ was added to the SiO_2 support. After an intermediate drying step, the cobalt nitrate solution (resp. nickel nitrate solution) was added to the support. All the samples were dried at 393 K and calcined at 623 K. The resulting oxidic precursors were reduced in pure H_2 or a flow of 4.8% H_2/Ar at a rate of 10 $ml\,min^{-1}$. Finally, the samples were passivated in a flow of 0.5% O_2/He (30 $ml\,min^{-1}$) for 2 h at room temperature. The passivated phosphides can be handled in air. $NiMo/Al_2O_3$ with 8 wt% Mo and 3 wt% Ni loadings was prepared by pore-volume impregnation of a γ-Al_2O_3 carrier (Condea, 210 $m^2\,g^{-1}$, particle size: 177–250 μm) using $(NH_4)_6Mo_7O_{24} \cdot 4H_2O$ and $Ni(NO_3)_2 \cdot 6H_2O$ salt solutions. The impregnated sample was dried at 393 K for 10 h and then calcined in air at 773 K.

2.2. Catalyst characterization

Temperature-programmed reduction experiments were carried out in a Micromeritics AutoChem 2910 apparatus. The sample (∼ 180 mg) was placed in a quartz U-shaped tube and reduced in a flow of a 4.8% H_2/Ar mixture (10 $ml\,min^{-1}$). The desired reduction temperature was reached at a rate of 5 $K\,min^{-1}$ for all the samples except

Table 1
Characteristics of the catalysts

Catalyst	Metal salt precursor	Metal loading (wt%)[a]	P loading (wt%)[a]	Molar ratio M:P[b] (M_0:P_0)[c]	S content (wt%)[a]
Co_2P/SiO_2	$Co(NO_3)_2 \cdot 6H_2O$	5.7 [0.8]	1.5 [0.2]	2:1 (2:1)	0.1
MoP/SiO_2	$(NH_4)_6Mo_7O_{24} \cdot 4H_2O$	8.3 [0.4]	3.1 [0.3]	1:1.2 (1:1.3)	0.15
WP/SiO_2	$(NH_4)_6H_2W_{12}O_{40} \cdot 18H_2O$	15.5 [1.4]	2.4 [0.3]	1.1:1 (1:1)	0.04
$NiMoP/SiO_2$	$(NH_4)_6Mo_7O_{24} \cdot 4H_2O$	4.6 [0.2]	1.7 [0.1]	2:1 (2:1)	0.25
	$Ni(NO_3)_2 \cdot 6H_2O$	3.7 [0.2]			
$CoMoP/SiO_2$	$(NH_4)_6Mo_7O_{24} \cdot 4H_2O$	4.2 [0.3]	1.5 [0.2]	2.1:1 (2:1)	0.1
	$Co(NO_3)_2 \cdot 6H_2O$	3.4 [0.3]			
$NiMo/Al_2O_3$[d]	$(NH_4)_6Mo_7O_{24} \cdot 4H_2O$	8		–	–
	$Ni(NO_3)_2 \cdot 6H_2O$	3		–	–

[a] Measured after HDN; numbers in brackets correspond to the standard deviation.
[b] M stands for the metals used in the corresponding phosphides: M = Co, Ni, W, or Mo.
[c] (M_0:P_0) = initial metal-to-P ratio introduced onto the support before reduction.
[d] Sulfidic sample.

for $NiMoP/SiO_2$ (2 K min^{-1}). Prior to the analyses, the temperature-programmed reduction of a reference material (silver oxide) was carried out using the same rates of flow and heating as those used for the phosphidic materials. The peak area of the reference material was correlated to the known volume of consumed H_2; these data were used to calculate H_2 consumption during the reduction of the phosphidic precursors.

XRD measurements were obtained using a Siemens D-5000 powder X-ray diffractometer (Cu-K_α radiation) with Bragg–Brentano geometry. The sample was pressed into a flat sample holder, which was rotated during the measurement. All the patterns were compared with calculated patterns (obtained from the Inorganic Crystal Structure Database) using the software PowderCell 2.3 [23]. The size of the supported crystalline metal phosphide was determined by applying the Scherrer equation, $D = 0.9\lambda/\beta\cos\theta$, where D is mean crystallite size (in nm), λ is wavelength of the X-ray radiation (in nm), β is full width at half-maximum (in radians), and θ is diffraction angle (in degrees).

^{31}P NMR spectra were measured with an Advance 400 WB Bruker spectrometer equipped with a magic-angle-spinning probe. The probe was tuned to 162 MHz, and an external sample of 85% phosphoric acid was used as the reference standard. Samples were packed into a 4-mm-diameter rotor and spun at 10 kHz. The spectra were obtained by applying the Fourier transformation to the free induction decay signals. Spectra were acquired using a single 1.6-μs pulse causing a flip angle of $\pi/4$ and a recycle time of 1 s. The measurements were performed at room temperature under in situ conditions, i.e., the samples were transferred from the synthesis reactor to the rotor in an inert atmosphere. The isotropic shifts of the signals were obtained by comparing spectra measured at different spinning rates.

Nitrogen adsorption isotherms were measured at 77 K using a Micromeritics Tristar 3000 instrument. The surface area was determined according to the BET method.

In a Micromeritics ASAP 2010 apparatus, CO chemisorption analyses were performed under static volumetric conditions, and the samples were re-reduced in situ in H_2 at 623 K prior to the measurements. The sample was evacuated at 573 K for 1 h and left to cool to 308 K. The chemisorption isotherm was obtained by measuring the adsorbed amount of CO for pressures varying from 10 to 600 mm Hg. Assuming a stoichiometry of one CO molecule per surface metal atom, the dispersion was calculated. After completing the initial analysis, the reversibly adsorbed gas was evacuated and the analysis repeated to determine the chemisorbed molecules only.

The element concentrations of P, Co, Mo, W, and Ni were determined by laser ablation-inductively coupled plasma mass spectrometry (LA-ICP-MS) [24]. The samples were pressed into pellets and analyzed directly by LA-ICP-MS using 80-μm ablation craters (2 Hz, 7 J cm^{-2}). We prepared two samples containing 98 wt% SiO_2 and 2 wt% P or 96 wt% SiO_2 and 4 wt% P to calibrate P with Si as the internal standardization element for correction of the different mass transport per sample. Furthermore, a NIST 610 reference glass was used for external standardization of P, Co, Mo, W, and Ni, where Si was also the internal standardization element. The samples were ablated for 60 s, acquired in transient mode, integrated, and processed according to the procedure described by Longerich et al. [25]. Table 1 presents the results and standard deviations, which were calculated from analyses of four replications of each sample.

The amount of sulfur in each sample after the HDN of OMA was determined by micro-elemental analysis: after oxidizing the samples at 1273 K in O_2, the amount of SO_2 produced was measured by IR.

2.3. HDN activity measurements

The catalytic tests for the HDN of *o*-methylaniline were carried out in a continuous-flow microreactor at a total pressure of 3.0 MPa. A sample of the catalyst under investigation (Table 2), diluted with 8 g SiC, was used for each reaction. To remove the oxygen from the surface of the passivated catalysts, the catalysts were activated in situ with H_2 at 673 K and 0.1 MPa for 3 h. The liquid reactant was fed into the reactor by means of a high-pressure pump using *n*-octane as the solvent. The catalyst was stabilized at 643 K and 3.0 MPa for at least 12 h before the samples were taken. Space-time was varied by changing the flow rate while the ratio between the liquid feed and the H_2 gas flow was constant. The reaction products were analyzed on-line with a Varian 3800 gas chromatograph equipped with a FID detector; *n*-heptane was used as the internal standard. Each set of experimental conditions was maintained for at least 3 h. The initial partial pressure of *o*-methylaniline was 3 kPa. The experiments were carried out in the absence of H_2S, in the presence of H_2S, and after removing H_2S from the feed. Adding dimethyl disulfide to the feed resulted in a partial pressure of 3 kPa for H_2S. Prior to the catalytic testing, $NiMo/Al_2O_3$ was sulfided in situ for 4 h at 673 K in a flow of 10% H_2S/H_2.

Table 2
Chemisorption results and turnover numbers for all the catalysts

Catalyst	Sample (g)	D (%)[a]	Surface metal atoms (μmol g^{-1} (sample))	OMA conversion (%)[b]	TON[b] 10^{-9} (mol s^{-1} μmol (active metal center)$^{-1}$)
Co_2P/SiO_2	1	0.50	4.8	45	11.2
MoP/SiO_2	0.7	0.40	3.5	26	12.7
WP/SiO_2	0.7	< 0.1	n.d.[c]	9	n.d.
$NiMoP/SiO_2$	1	1.05	11.6	25	2.6
$CoMoP/SiO_2$	1	0.45	4.7	25	6.4
$NiMo/Al_2O_3$	0.05	–	332.2[d]	36	2.6

[a] Metal dispersion as determined by CO chemisorption.
[b] Determined for a flow rate of OMA $= 1.2 \times 10^{-7}$ mol(OMA) s^{-1}.
[c] n.d., not determined.
[d] Number of edge Mo centers.

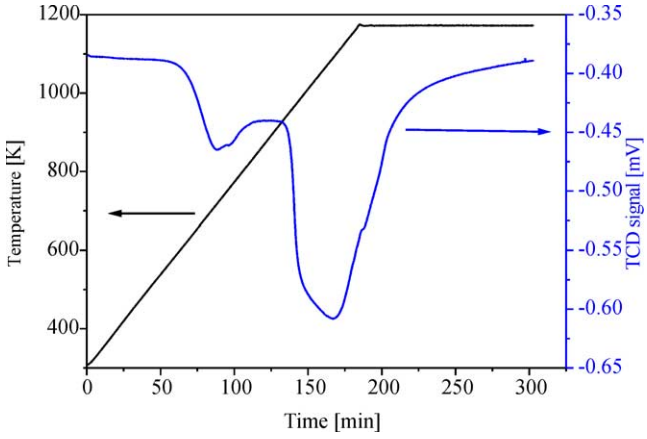

Fig. 1. TPR of MoP/SiO_2.

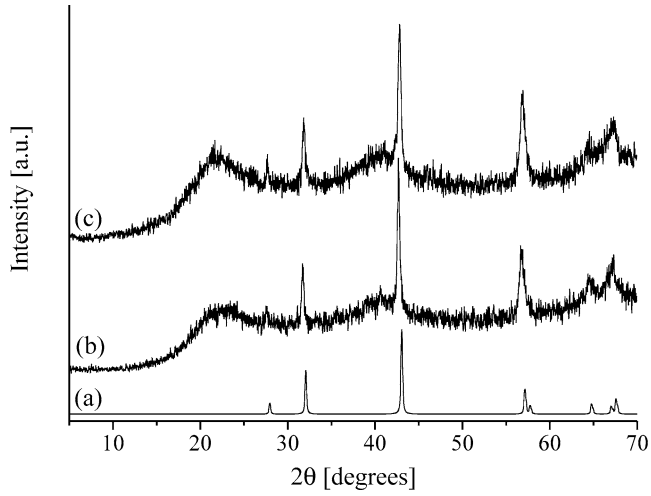

Fig. 2. Powder XRD patterns of MoP/SiO_2: simulated (a) before HDN (b) and after HDN (c).

3. Results and discussion

3.1. MoP/SiO_2

For the synthesis of MoP/SiO_2, Mo and P were added to the support by pore-volume impregnation of an aqueous solution, obtained by mixing a Mo salt, $(NH_4)_6Mo_7O_{24} \cdot 4H_2O$, with $(NH_4)_2HPO_4$. After calcination, it was assumed that the Mo and P species were present on the support in a high oxidation state: Mo^{6+} and P^{5+}, respectively. The oxidic precursor was then reduced in a flow of 4.8% H_2 in Ar (10 ml min^{-1}); the temperature was increased with a linear ramp of 5 K min^{-1} until 1173 K, which was maintained for 2 h. Fig. 1 shows the TPR profile with two main peaks with maxima at 720 and 1090 K. The peak at 720 K is assigned to the reduction of Mo^{6+} species to Mo^{4+} [26], while the large peak at 1090 K is assumed to result from the overlapping of the different peaks, corresponding to the reduction of Mo^{4+} to Mo^0 on the one hand and of P^{5+} to P^0 on the other. The total reduction process (for an equimolar amount of Mo and P) is represented by the following equation:

$$2MoO_3 \cdot P_2O_5 + 11H_2 \rightarrow 2MoP + 11H_2O.$$

Our sample (181 mg) contained 157 μmol Mo and 204 μmol P. The peak area of the TPR profile (Fig. 1) corresponds to the consumption of 960 μmol H_2. Assuming a total reduction of Mo^{6+} to Mo^0 (which corresponds to a consumption of 471 μmol H_2), 489 μmol H_2 was used for the reduction of the phosphate species. Since a total reduction of 204 μmol P^{5+} to P^0 requires 510 μmol H_2, the TPR results indicate that approximately 4% of the phosphate introduced onto the SiO_2 support was not reduced. Species in intermediate oxidation states may have formed during the reduction process.

As P compounds (P_2O_5, reduced P) are volatile, an elemental analysis of the reduced phosphide samples was carried out to determine whether P was lost during the reduction process (Table 1). To prepare MoP/SiO_2, an excess of P (compared to the stoichiometry of the molybdenum phosphide of 1 to 1) was introduced onto the support with a Mo-to-P ratio of 1 to 1.3. The elemental analysis of the MoP/SiO_2 sample after reduction at 1173 K indicated an excess of P with a Mo-to-P ratio of 1 to 1.2 (RSD for P measurements = 10–15%). This suggests that, despite the high reduction temperature, only small amounts of P were lost during the process. Similar features were observed with the other transition-metal phosphides (Table 1), for which the metal(s)-to-P ratio after reduction was very close to the nominal M:P ratio.

The temperature-programmed reduction of Co_2P/SiO_2, $CoMoP/SiO_2$, and $NiMoP/SiO_2$ was also carried out in a flow of 4.8% H_2/Ar (10 ml min^{-1}). The reduction temperature of 1173 K was reached at a rate of 5 K min^{-1} for the Co-containing samples and of 2 K min^{-1} for $NiMoP/SiO_2$. The TPR profiles confirmed the reduction of the metal(s) and phosphorus (not shown). The TPR apparatus is equipped with a thermal conductivity detector, which requires a gas mixture (H_2/Ar in our case) to be able to measure the H_2 consumption during the temperature-programmed reduction. As the preparation of WP/SiO_2 was carried out in pure H_2, a TPR profile was not recorded for the reduction of the precursor of WP/SiO_2.

Powder XRD confirmed the formation of MoP on the SiO_2 support (Fig. 2). Six reflections corresponding to crystalline MoP are visible in the XRD pattern measured after reducing and passivating the sample (Fig. 2b) [27]. A broad reflection at 2θ of 40° is also detected on the pattern. This is due either to small MoP particles or, more likely, to small metallic molybdenum particles, the planes (110) of which give rise to a 2θ reflection at 40°.

Molybdenum phosphide crystallizes in the hexagonal tungsten carbide (WC) structure with only one P site, at which six Mo atoms surround the P atom trigonal prismatically. Fig. 3 represents the ^{31}P MAS NMR spectra obtained for MoP/SiO_2 treated under different conditions at a spinning rate of 10 kHz. The main signal, with an isotropic shift centered at 214 ppm and corresponding to MoP, was de-

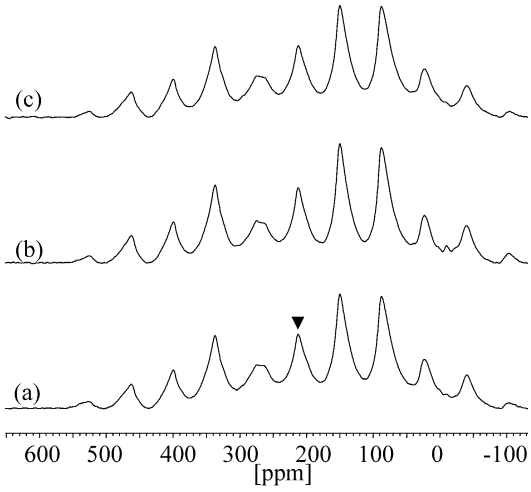

Fig. 3. ^{31}P MAS NMR spectra of MoP/SiO_2 after reduction at 1173 K (a), after reduction at 1173 K, passivation at room temperature, and exposure to air (b), and after reduction at 1173 K, passivation, exposure to air, and re-reduction at 673 K (c).

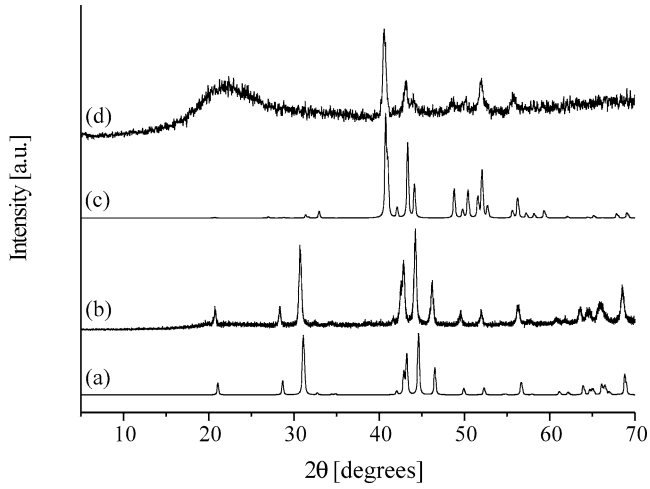

Fig. 4. Powder XRD patterns of WP/SiO_2, simulated (a) and experimental (b); and of Co_2P/SiO_2, simulated (c) and experimental (d).

tected after reduction at 1173 K (Fig. 3a). The measurement was carried out in the absence of air; a small shoulder, typical of phosphate species, was detected at −10 ppm [28,29]. The NMR spectrum of MoP/SiO_2 after reduction at 1173 K, passivation at room temperature and exposure to air is shown in Fig. 3b. The increased intensity of the small peak at −10 ppm indicates that oxidation of the sample took place upon exposure to air. The intensity of this peak, typical of phosphate, decreased after re-reduction at 673 K in pure H_2 (Fig. 3c), indicating that the oxidation of the sample upon exposure to air was a reversible phenomenon. Those chemical shifts are comparable to those reported by Clark et al. [30], who found a chemical shift of 214 ppm for bulk MoP and of 199 ppm for SiO_2-supported MoP when the samples were measured in situ. For the latter sample, a relatively broad peak, corresponding to phosphate species, was also detected on the support. The isotropic shift observed for MoP/SiO_2 results from the metallic conductivity of the transition-metal phosphide due to the strong metal–metal bonding in those compounds. The conduction electrons interact with the nucleus producing a high-frequency shift known as the Knight shift.

3.2. WP/SiO_2

The synthesis of WP/SiO_2 was first attempted with a reduction mixture of 4.8% H_2 in Ar and at a flow rate of 10 ml min^{-1}. Contrary to the other supported phosphides investigated, no phosphide of tungsten was detected by XRD at reduction temperatures up to 1273 K. The reduction was then carried out at the same temperature (1273 K) in pure H_2 and the XRD pattern of the resulting material is shown in Fig. 4b. Sharp peaks indicate the presence of large WP particles, probably due to sintering under the high reduction temperature.

WP crystallizes in the MnP structure, in which six W atoms form a distorted trigonal prism around the P atoms. The ^{31}P MAS NMR spectrum obtained for WP/SiO_2 (Fig. 5a) is in agreement with the results reported for bulk materials [30,31]. There was an isotropic shift of 255 ppm. As for the case of MoP/SiO_2, this Knight shift is caused by the metallic character of WP.

3.3. Co_2P/SiO_2

For the preparation of the SiO_2-supported cobalt phosphide, the influence of the Co-to-P ratio was investigated. Samples with Co-to-P ratios varying from 1.5 to 0.5 were prepared. Fig. 4d shows that Co_2P was the only crystalline phase detected for the sample with a Co:P ratio of 2:1.3. Although a number of impurities were detected in the samples with Co-to-P ratios of 1 and 0.5, Co_2P was the main

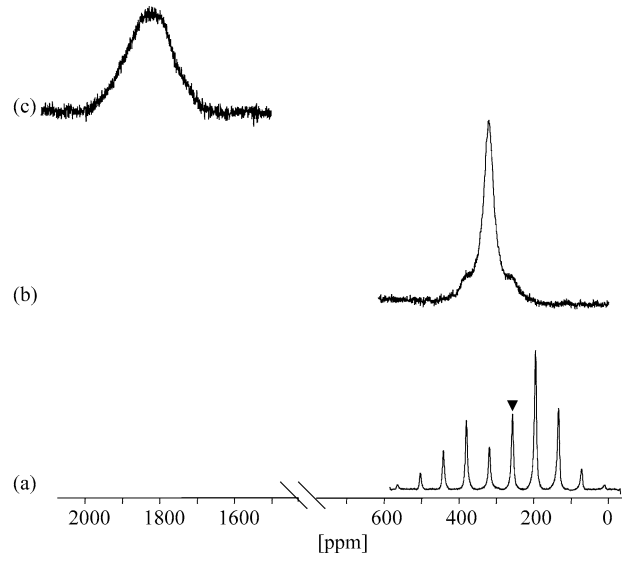

Fig. 5. ^{31}P MAS NMR spectra of WP/SiO_2 (a), $CoMoP/SiO_2$ (b), and Co_2P/SiO_2 (c) at a spinning rate of 10 kHz.

phosphorus-containing phase detected by XRD (not shown). Under these conditions, Co_2P seems to be the most stable phosphide phase formed on SiO_2. These results differ from those reported by Wang et al. [32], who detected the presence of the cobalt monophosphide CoP on silica, when the Co-to-P ratio was 1.

Solid-state NMR of samples containing Co species is complicated due to the paramagnetism of the Co cations. Paramagnetic interactions between the Co species and the resonant nucleus may induce shorter relaxation delays, a decrease in the intensity of the signal and line broadening, thus resulting in more complex spectra [33]. Fig. 5c shows the ^{31}P MAS NMR spectrum for Co_2P/SiO_2. Co_2P crystals have an orthorhombic Co_2Si structure, in which the phosphorus is surrounded by Co atoms in a tricapped trigonal prismatic environment [34]: each P is surrounded by six Co atoms, which form a trigonal prism, and each of the three faces of the prism is capped by another Co atom. As in all the other phosphide structures, strong metal–metal bonding occurs in Co_2P due to the short Co–Co distances. This results in metallic conductivity and high values of the NMR shifts for phosphide materials, very different from those observed for phosphate species. In addition to the broadening of the signal, a high Knight shift of 1830 ppm was observed for the cobalt phosphide sample supported on SiO_2, in agreement with the shift of 1839 ppm measured for bulk Co_2P [31].

3.4. $CoMoP/SiO_2$

The addition of Co or Ni to Al_2O_3-supported molybdenum sulfide catalysts promoted the activity of these materials in hydrotreating reactions. To determine whether it is possible to induce a promotional effect by adding Co and/or Ni to a SiO_2-supported MoP, the ternary compounds CoMoP and NiMoP were synthesized.

The XRD pattern corresponding to $CoMoP/SiO_2$ (Fig. 6b) confirms the successful preparation of the ternary phosphide phase on a support. CoMoP crystals have the same type of

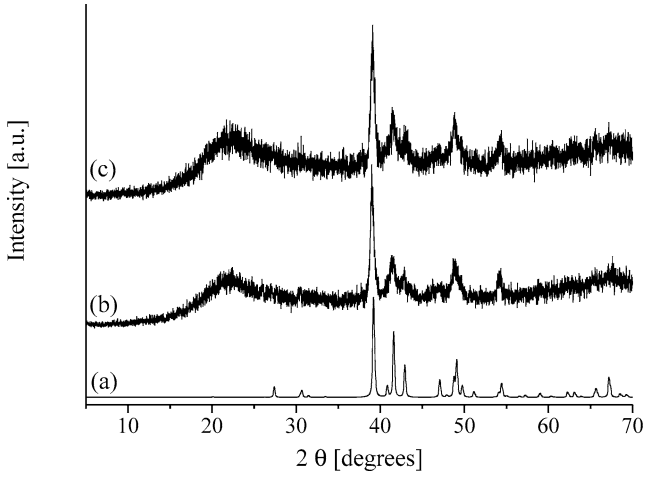

Fig. 6. Powder XRD patterns of $CoMoP/SiO_2$: simulated (a) before HDN (b) and after HDN (c).

Table 3
Phosphide structures and ^{31}P MAS NMR results

Catalyst	Structure type	δ_{iso}[a] (ppm)	FWHM[b] (kHz)
Co_2P/SiO_2	Co_2Si	1830	25
MoP/SiO_2	WC	214	3.2
WP/SiO_2	MnP	255	1.3
$NiMoP/SiO_2$	Fe_2P	–	–
$CoMoP/SiO_2$	Co_2Si	320	5.5

[a] δ_{iso}, isotropic chemical shift.
[b] FWHM, full width at half-maximum.

structure as Co_2P (i.e., Co_2Si), with half of the Co atoms being replaced by Mo atoms in an ordered fashion [35]. As in Co_2P, only one crystallographic P site exists. Fig. 5b shows the ^{31}P MAS NMR spectrum for $CoMoP/SiO_2$, with a Knight shift of 320 ppm and shoulders on both sides of the isotropic shift, corresponding to sidebands. As for Co_2P/SiO_2, the line width of the $CoMoP/SiO_2$ sample was bigger than that of the MoP sample. The presence of Mo reduced the number of interactions between the paramagnetic Co center and the resonant P nucleus, shifting the Knight shift to lower values and reducing the width of the NMR signal compared to that of the binary cobalt phosphide Co_2P. Since crystals of Co_2P and CoMoP have the same type of structure, their electron density may be the same and the Knight shift might be proportional to the susceptibility [36]. In that case, the difference in the Knight shift between Co_2P and CoMoP might be due to the difference in Pauli susceptibility of the two compounds (6.25×10^{-4} emu mol^{-1} for Co_2P and 1.67×10^{-4} emu mol^{-1} for CoMoP [37]).

Table 3 lists the structure types of the metal phosphides and the ^{31}P NMR results. The broadening effect, induced by the presence of the paramagnetic Co, is highlighted by the values of the full width at half-maximum for each phosphide: while full width at half-maximum values of 1.3 kHz for WP/SiO_2 and 3.2 kHz for MoP/SiO_2 were obtained, these values increased to 5.5 kHz for the ternary phosphide $CoMoP/SiO_2$ and to 25 kHz for Co_2P/SiO_2, indicating strong interactions between the ^{31}P nucleus and the Co centers. The ^{31}P NMR experiments also revealed small amounts of unreduced phosphate species on $CoMoP/SiO_2$, $NiMoP/SiO_2$, and Co_2P/SiO_2 (not shown) with peaks of chemical shifts between -10 and 5 ppm. In contrast, unreduced phosphates were not detected on WP/SiO_2, probably due to the higher reduction temperature (1273 K instead of 1173 K).

3.5. $NiMoP/SiO_2$

The ternary phosphide $NiMoP/SiO_2$ was also synthesized, although a small amount of an unidentified crystalline phase was also detected in the XRD pattern (Fig. 7b). Compared to the other transition-metal phosphides prepared, the width and the low resolution of the XRD reflection peaks show that small NiMoP particles were obtained on the SiO_2 carrier. The particle size of the phosphide phases was es-

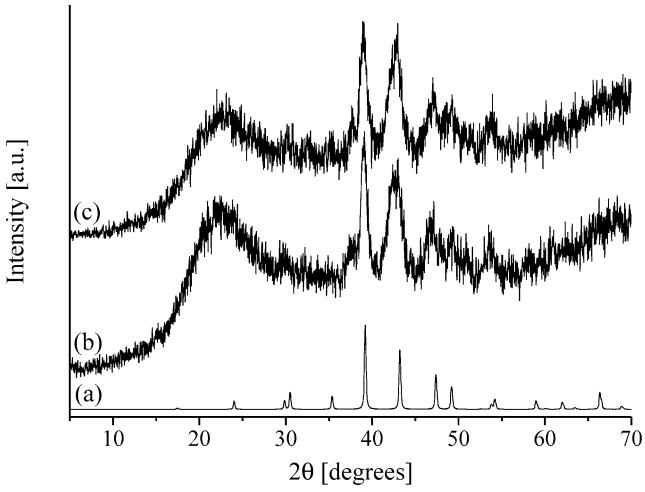

Fig. 7. Powder XRD patterns of $NiMoP/SiO_2$: simulated (a) before HDN (b) and after HDN (c).

timated from the XRD patterns by applying the Scherrer equation (Table 4). While crystallites as big as 27 nm were present on SiO_2 for the tungsten phosphide sample, particles of around 8 nm were detected for NiMoP. As reported above, this difference is probably due to the strong reduction conditions used in the case of WP/SiO_2. For MoP/SiO_2, Co_2P/SiO_2, and $CoMoP/SiO_2$, the preparation conditions (i.e., reduction temperature, flow rate, H_2 concentration in the feed) were similar to those used for $NiMoP/SiO_2$, with the exception of the heating rate (2 $K\,min^{-1}$ for $NiMoP/SiO_2$ as opposed to 5 $K\,min^{-1}$). There was a clear difference in the crystallite size of the MoP, CoMoP, and Co_2P particles (15–18 nm) compared to the 8 nm of the NiMoP crystallites. The slower heating rate and/or the presence of Ni species seem to have a positive effect on the dispersion of the NiMoP particles. Interactions may take place between the Ni and the SiO_2 support, thus preventing sintering.

NiMoP crystals have a Fe_2P structure, with two crystallographic sites for P: a tricapped trigonal prism $P(Ni_6Mo_3)$ and a tricapped trigonal prism $P(Ni_3Mo_6)$. Two signals, corresponding to each P site, should have been visible in the NMR spectrum of the $NiMoP/SiO_2$ sample, but none were detected in the investigated frequency range (−500 to 5000 ppm). This differs from the results reported by Wada et al. [38], who performed their measurements under static conditions and detected a single signal at 70 ppm. ^{31}P MAS NMR measurements were also carried out for a bulk NiMoP sample under the same conditions as reported here [31]. A poorly resolved signal was detected for NiMoP at 97 ppm, while a signal corresponding to MoP, present as an impurity in this sample, was also detected, its sidebands overlapping with the NiMoP signal. The absence of a signal during our measurements may result from a number of factors: (i) the relatively low loading of phosphide on the support and, hence, the small amount of NiMoP in the rotor, and (ii) a broadening of the signal due to the presence of the paramagnetic Ni center, resulting in its disappearance.

Table 4
BET surface areas and mean size of metal phosphide crystallites

Catalyst	BET surface area ($m^2\,g^{-1}$)	Metal crystallite size[a] (nm) (hkl)[b]
SiO_2	500	–
SiO_2 red. 1173 K	320	–
2 wt% P/SiO_2 red. 1173 K	78	–
Co_2P/SiO_2	120	18 (112)
MoP/SiO_2	80	15 (101)
WP/SiO_2	120	27 (103)
$NiMoP/SiO_2$	256	8 (111)
$CoMoP/SiO_2$	158	15 (112)

[a] Calculated according to the Scherrer equation.
[b] Miller indices of the XRD line from which the crystallite sizes were calculated.

3.6. Activity measurements

The activity of the catalysts was tested in the HDN of *o*-methylaniline at 643 K and 3.0 MPa. Prior to the measurements of the catalytic activity, the sample was reactivated in situ in a flow of H_2 for 2 h at 673 K. In the case of the reference $NiMo/Al_2O_3$ sulfidic material, the sample was sulfided in situ for 4 h at 673 K in a flow of 10% H_2S/H_2 prior to catalytic testing. The influence of H_2S on the reaction was studied by introducing 3 kPa of dimethyl disulfide into the feed. All the phosphides displayed some activity in the HDN of *o*-methylaniline. Fig. 8 shows the activity over MoP/SiO_2, which increased with increasing space-time and leveled off at higher space-time. In the presence of H_2S, the activity of MoP/SiO_2 decreased slightly, while after the removal of H_2S, the activity was higher than it was before the introduction of H_2S. The influence of Co and Ni, together with molybdenum in the phosphide phase, on the activity of those materials was also studied. Figs. 9 and 10 give the activity measurements of $CoMoP/SiO_2$ and $NiMoP/SiO_2$.

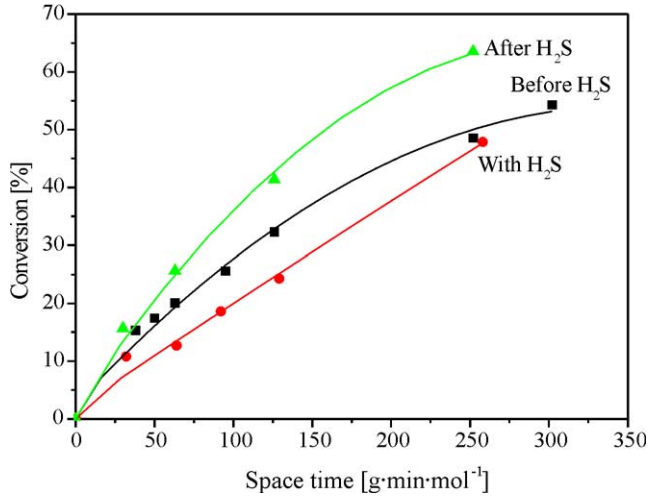

Fig. 8. HDN conversion of *o*-methylaniline over MoP/SiO_2 in the absence of H_2S, in the presence of H_2S, and after removal of H_2S.

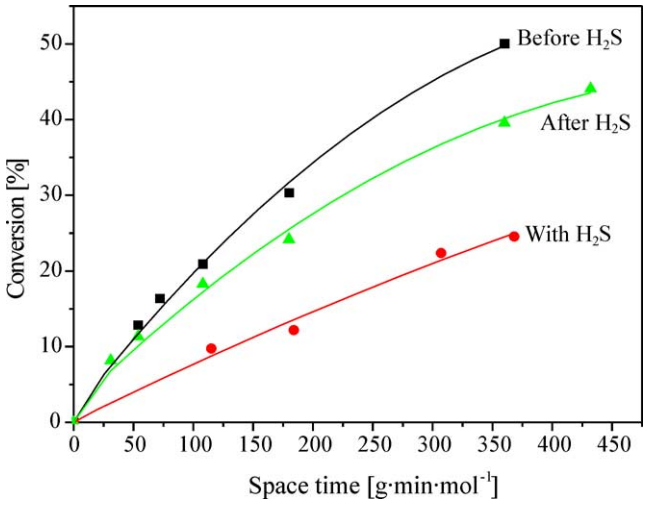

Fig. 9. HDN conversion of *o*-methylaniline over $CoMoP/SiO_2$ in the absence of H_2S, in the presence of H_2S, and after removal of H_2S.

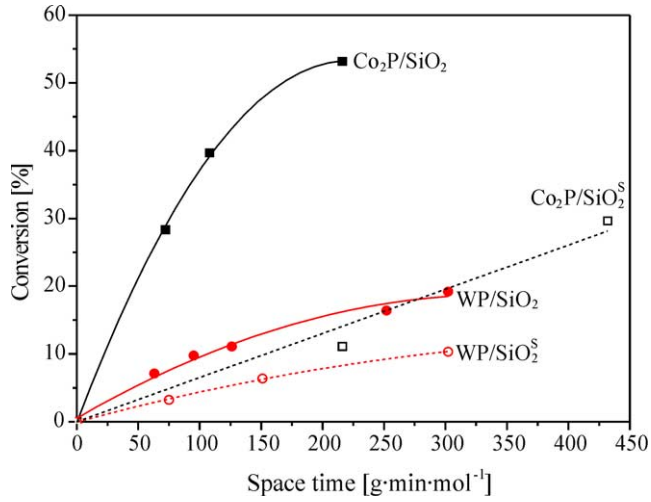

Fig. 11. HDN conversion of *o*-methylaniline over Co_2P/SiO_2 and WP/SiO_2 in the absence (closed symbols) and presence of H_2S (open symbols).

The presence of H_2S lowered the HDN activity of both materials. After removing H_2S, the activities of $CoMoP/SiO_2$ and $NiMoP/SiO_2$ increased but not to their original levels. Fig. 11 shows the activities over Co_2P/SiO_2 and WP/SiO_2 in the absence and presence of H_2S; both materials were active. The two catalysts cannot be directly compared, however, because the amount and the dispersion of the samples were different: 1 g Co_2P/SiO_2 (dispersion = 0.5%) and 0.7 g WP/SiO_2 (with a dispersion below 0.1%) were loaded into the reactor. The dispersion for WP/SiO_2 was very low and, thus, the turnover number of this material could not be calculated. As in the case of the Mo-containing phosphides, the presence of H_2S strongly inhibited the HDN of OMA over Co_2P/SiO_2 and WP/SiO_2. The decrease in the activity of all the phosphidic materials in the presence of H_2S was explained by the competitive adsorption of H_2S on the catalyst surface, which blocked the active sites. The increase in the activity observed over MoP/SiO_2 after the removal of H_2S (Fig. 8) may have been caused by the development of new active sites or/and the modification of existing sites, induced by the presence of H_2S. However, XRD measurements of the MoP/SiO_2 sample after the HDN reaction did not reveal a difference in the XRD pattern compared to the pattern before HDN (Fig. 2). This similarity in the two XRD patterns is probably due to the fact that the restructuring, which leads to the higher activity of the MoP/SiO_2 sample after the removal of H_2S, is on the one hand, a surface phenomenon, and, on the other, occurs on small or/and amorphous particles. This would, then, explain why the restructuring of the catalyst is not revealed by XRD. The higher performance of the SiO_2-supported MoP after the removal of H_2S may be due to small active MoS_2 particles, which may form upon H_2S sulfidation of small Mo particles present on the silica carrier together with MoP.

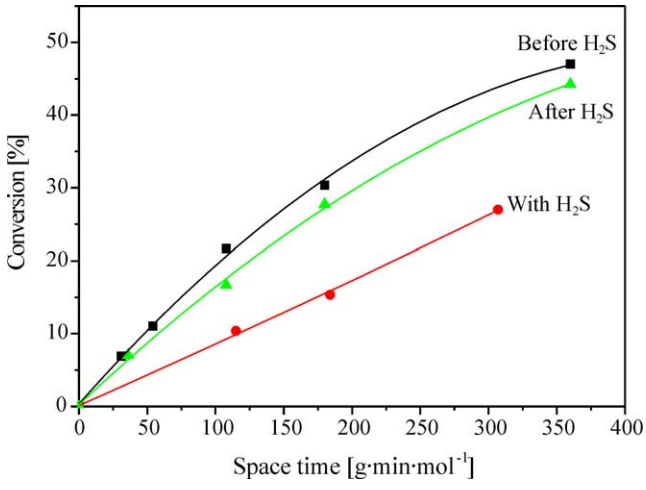

Fig. 10. HDN conversion of *o*-methylaniline over $NiMoP/SiO_2$ in the absence of H_2S, in the presence of H_2S, and after removal of H_2S.

Figs. 6c and 7c present the XRD patterns of $CoMoP/SiO_2$ and $NiMoP/SiO_2$ after HDN. These patterns were compared to the XRD patterns of the same samples before HDN; no difference was detected. X-ray diffractograms, similar to those measured right after reduction, were also obtained for Co_2P/SiO_2 and WP/SiO_2 after the HDN reaction (not shown). This indicates that, once formed, the phosphide phases are probably stable, even in the presence of H_2S. Elemental analysis of S was performed for the different SiO_2-supported metal phosphides after HDN (Table 1). 0.04 wt% S was detected on the WP/SiO_2 sample, while 0.25 wt% S was detected on the $NiMoP/SiO_2$ sample. The Co-containing phosphides, namely Co_2P/SiO_2 and $CoMoP/SiO_2$, each contained 0.1 wt% S after HDN, while MoP/SiO_2 contained 0.15 wt% S. The differences are quite significant, but we could not determine the type of sulfur present in the sample. Physisorbed H_2S could be present both on the support and on the metal phosphide particles, and surface sulfidation of the metal phosphides may also have taken place. The sulfur-to-active site (based on CO chemisorption) ratio was 7 mol mol^{-1} for Co_2P/SiO_2,

$CoMoP/SiO_2$, and $NiMoP/SiO_2$, and 14 mol mol^{-1} for MoP/SiO_2. A direct correlation, however, was not found between these values and the stability of the phosphidic materials in the presence of H_2S. MoP/SiO_2 had the highest S to active site ratio after HDN and the smallest loss of activity in the presence of H_2S. The transition metal phosphides Ni_2P and Co_2P were prepared under hydrotreating conditions from Ni and Co precursors containing phosphates [8,39]. Robinson et al. [8] and Korányi [39] also reported that $NiPS_3$ decomposes to Ni_2P, even in the presence of H_2S. This supports the assumption that the transition-metal phosphides are stable even under hydrotreating conditions.

CO chemisorption experiments were carried out to determine the active metal surface area of the phosphidic materials, assuming a stoichiometry of one CO molecule per surface metal atom. This enabled us to compare the activity of the catalysts. Table 2 lists the results and the normalized activities as turnover numbers. If only one of the two types of metal atoms at the surface of CoMoP and NiMoP is catalytically active and if both adsorb CO, then our turnover numbers for these bimetallic phosphides may be underestimated by a factor two. The dispersion of the metal phosphide was quite low in all the materials. $NiMoP/SiO_2$ had the highest dispersion (1.0%), while the dispersion in WP/SiO_2 was too low ($< 0.1\%$) to report it without a large margin of error. MoP/SiO_2, $CoMoP/SiO_2$, and Co_2P/SiO_2 had similar dispersion values (0.40, 0.45, and 0.5%, respectively). This trend observed for the dispersion values is in agreement with the results reported above for the mean crystallite size determined from the XRD patterns and the Scherrer equation: WP/SiO_2 had large particles (27 nm) and very low dispersion ($< 0.1\%$), while the contrary was observed for $NiMoP/SiO_2$ (8 nm and 1.0%, respectively). The dispersion values were, however, much lower than expected from the size of the particles. Assuming that the active particles have a regular geometry (sphere, for instance), the particle size can be estimated using

$$d = (6/(A_{\mathrm{Sm}} D\rho)) \times 100,$$

with d being the particle diameter (in nm), A_{Sm} the metallic surface area (in $m^2\,g_{metal}$), D the dispersion (in %), and ρ the metal density. The metallic surface area (A_{Sm}) and the dispersion (D) were obtained from the CO chemisorption experiments. Using this equation and the results obtained by CO chemisorption, particle sizes of approximately 110 nm for MoP/SiO_2, 63 nm for $CoMoP/SiO_2$, 60 nm for Co_2P/SiO_2, and 12 nm for $NiMoP/SiO_2$ were calculated. These values are higher than those obtained from the XRD results (Table 4). This may be due to the following: (i) P atoms are probably located at the surface of the phosphide particles and do not chemisorb any CO molecules. This would result in a lower dispersion than that obtained for a particle of similar size containing metal atoms only. (ii) The phosphidic materials investigated had a great loss surface area (Table 4). This loss was also observed for SiO_2 reduced at 1173 K (320 $m^2\,g^{-1}$) and P/SiO_2 reduced at 1173 K (78 $m^2\,g^{-1}$). The presence of P_2O_5 in silica causes shrinkage by forming phosphosilicate above 873 K and this may explain the great loss of surface area observed for P/SiO_2. In the phosphide-containing samples, the surface area varied from 80 to 256 $m^2\,g^{-1}$ depending on the metal on the support. The phosphide particles are, thus, probably embedded in the silica support, after the treatment under strong reduction conditions, thus making them inaccessible to CO molecules during the chemisorption experiments or to any gas molecules during the HDN experiments.

The turnover numbers were calculated for experiments carried out under the same reaction conditions (643 K, 3.0 MPa, flow rate $= 1.2 \times 10^{-7}$ mol(OMA) s^{-1}), taking into account the accessible metal surface centers in each phosphidic sample, as determined by CO chemisorption and the OMA conversion measured under the chosen conditions. Based on the following assumptions, the number of active surface metal centers of the sulfidic $NiMo/Al_2O_3$ was estimated: (i) Mo edge atoms are the catalytically active sites and (ii) hexagonal MoS_2 platelets with a diameter of approximately 25 Å are present on the Al_2O_3 support, as proposed by Shido and Prins on the basis of EXAFS measurements [40]. This results in 2.0×10^{20} Mo edge centers per gram of $Ni–Mo–S/Al_2O_3$ catalyst. MoP/SiO_2 and Co_2P/SiO_2 had the highest intrinsic activities and performed better than a classical sulfidic $NiMo/Al_2O_3$ catalyst (last column in Table 2). MoP/SiO_2 and Co_2P/SiO_2 were approximately twice as active as $CoMoP/SiO_2$; the intrinsic activity of $NiMoP/SiO_2$ was five times lower than that of MoP/SiO_2. The activity of the ternary phosphides $CoMoP/SiO_2$ and $NiMoP/SiO_2$ was about as high as that of the sulfidic $NiMo/Al_2O_3$ catalyst. Contrary to the sulfidic materials, for which the addition of Co or Ni to MoS_2 phases promotes the hydrotreating activity [1–3], the presence of Co or Ni together with Mo in the phosphidic catalysts did not have a beneficial effect on the activity of these materials.

3.7. Product selectivities

The main products of reaction obtained during the HDN of *o*-methylaniline over the phosphidic materials were methylcyclohexene (MCHE), methylcyclohexane (MCH), toluene (TOL), and ethylcyclopentane (ECP). With regard to the product distribution, the metal phosphides resemble sulfidic materials [41] and differ from nitrides, which yield significant amounts of hydrogenolysis products and are, thus, more similar to metallic catalysts [42]. Fig. 12 presents the reaction network of the HDN of *o*-methylaniline over sulfidic materials. Toluene and methylcyclohexylamine (MCHA) are the primary products of reaction and are formed through C–N bond hydrogenolysis and hydrogenation of the aromatic ring, respectively. Under our reaction conditions, MCHA was not detected but reacted further to form either MCHE by β-Hoffmann elimination or MCH. Rota and Prins [43] showed that an intermediate thiol compound was present in the HDN of methylcyclohexylamine

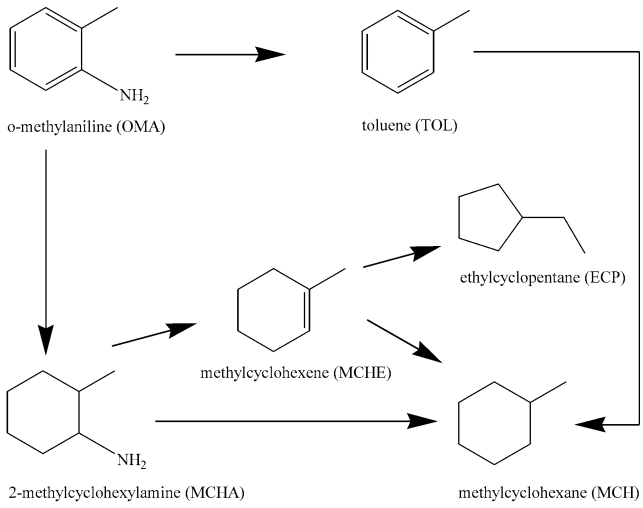

Fig. 12. HDN reaction network of *o*-methylaniline.

over sulfidic materials, indicating that MCHA could form MCH either by direct C–N bond hydrogenolysis or by nucleophilic substitution of the amino group of MCHA by an SH group followed by C–S bond hydrogenolysis. MCHE can also undergo further rearrangement to ECP.

Fig. 13 shows the plots of the product selectivity as a function of conversion in the presence and absence of H_2S for MoP/SiO_2. MCHE was the main reaction product and its selectivity and that of TOL decreased with increasing conversion, whereas the selectivity to MCH and ECP increased with increasing conversion. These results differ from those obtained in the HDN of *o*-propylaniline over sulfided Mo/Al_2O_3 in the absence of H_2S [44]. Over Mo/Al_2O_3, the order of selectivity was propylbenzene > propylcyclohexene > propylcyclohexane. The results obtained over MoP/SiO_2 are more similar to those obtained over Mo/Al_2O_3 in the presence of H_2S, for which the order of selectivity was propylcyclohexene > propylbenzene > propylcyclohexane [44]. In contrast to the sulfidic materials [41], for which MCH did not form by hydrogenation of TOL when OMA was present (because of inhibition of the adsorption of TOL by OMA), the hydrogenation of TOL appears to be a second possible route for the formation of MCH over phosphidic catalysts. The selectivity to MCHE and, to a lesser extent, the selectivity to TOL decreased in the presence of H_2S, while the selectivity to MCH increased. On the other hand, the total activity decreased in the presence of H_2S, which means that even smaller amounts of MCHE and TOL formed, while the amount of MCH remained constant. This suggests that H_2S inhibits the C–N bond hydrogenolysis and the hydrogenation of the aromatic ring of OMA. Figs. 14 and 15 give the selectivities for the same reaction over $CoMoP/SiO_2$ and $NiMoP/SiO_2$, respectively. Trends similar to those observed over MoP/SiO_2 were detected over $CoMoP/SiO_2$ and $NiMoP/SiO_2$: the main reaction product was MCHE followed by TOL. Over $CoMoP/SiO_2$, the selectivity and yield of MCHE increased, while less MCH

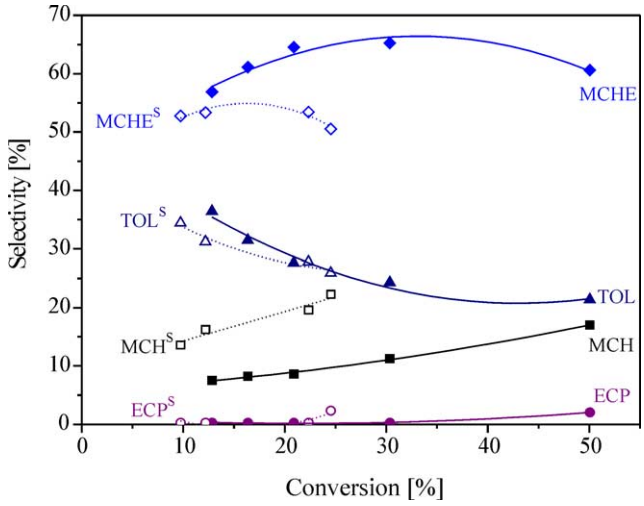

Fig. 14. Product selectivities of the HDN of *o*-methylaniline over $CoMoP/SiO_2$ in the absence (closed symbols) and presence of H_2S (open symbols).

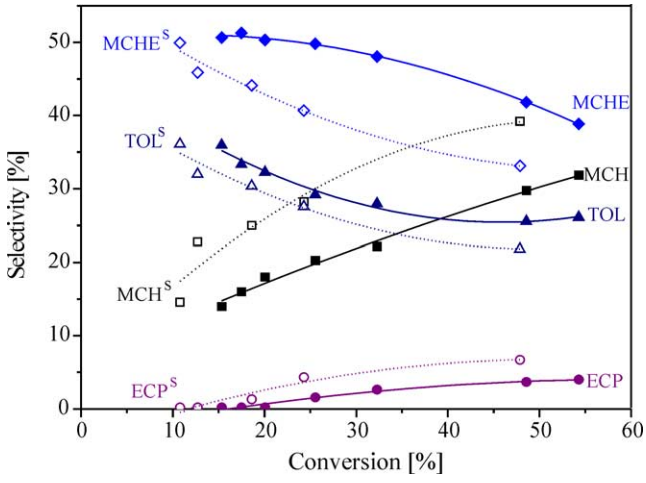

Fig. 13. Product selectivities of the HDN of *o*-methylaniline over MoP/SiO_2 in the absence (closed symbols) and presence of H_2S (open symbols).

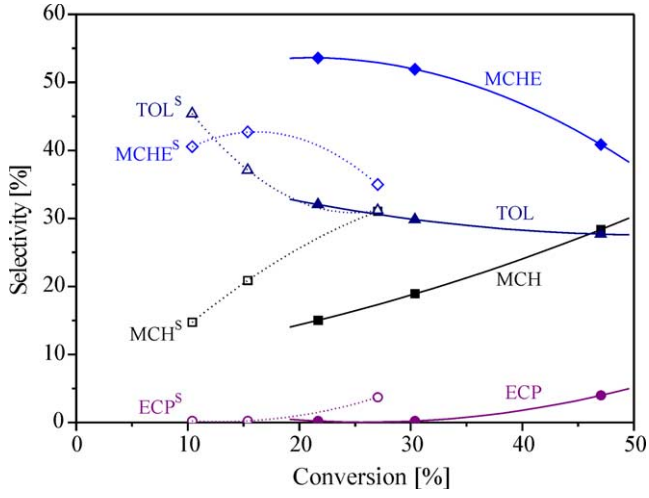

Fig. 15. Product selectivities of the HDN of *o*-methylaniline over $NiMoP/SiO_2$ in the absence (closed symbols) and presence of H_2S (open symbols).

formed compared to MoP/SiO_2, indicating that the presence of Co favors the elimination pathway from MCHA to MCHE. The presence of Ni in the $NiMoP/SiO_2$ sample, however, did not affect the product distribution compared to MoP/SiO_2. Similar to MoP/SiO_2, the presence of H_2S inhibited the formation of MCHE and, to a lesser extent, that of TOL during the HDN of OMA over $CoMoP/SiO_2$ and $NiMoP/SiO_2$.

The influence of H_2S on the activity and selectivity of the phosphidic materials differs from that observed over sulfidic Mo/Al_2O_3 and $NiMo/Al_2O_3$. As observed for the phosphidic catalysts, the conversion of *o*-propylaniline on the sulfidic materials is lower in the presence than in the absence of H_2S [44]. However, while the influence of H_2S on activity is moderate over MoP/SiO_2 (Fig. 8), the conversion is reduced by a factor three over sulfided Mo/Al_2O_3. The influence of H_2S on selectivity is very different. Thus, over the sulfidic materials, the propylbenzene selectivity in the HDN *o*-propylaniline decreased by a factor of two, and the propylcyclohexene selectivity increased by almost a factor of two upon addition of H_2S [44]. In this respect, the changes in selectivity, observed upon the introduction of H_2S over the phosphidic catalysts (Figs. 13–15), are considered minor. At the same time, this difference demonstrates that the catalytic performance of the phosphidic materials in the presence of H_2S cannot be due to MoS_2.

The HDN network of OMA over transition-metal phosphides is similar to that observed over sulfidic materials in the sense that no hydrogenolysis products form over both types of materials. Differences in the activity of these materials are, however, observed: (i) the direct hydrogenation of TOL appears to be a feasible route for the formation of MCH over the phosphidic samples, even in the presence of OMA and, (ii) the presence of H_2S inhibits the formation of MCHE over the phosphidic materials.

4. Conclusions

A variety of silica-supported transition metal phosphides (Co_2P/SiO_2, MoP/SiO_2, WP/SiO_2, $CoMoP/SiO_2$, and $NiMoP/SiO_2$) were prepared by temperature-programmed reduction of their corresponding metal oxide/phosphate precursor. ^{31}P MAS NMR spectroscopy is a powerful technique for the characterization of such compounds: Knight shifts of 214 and 255 ppm were observed for MoP and WP, respectively. In the presence of paramagnetic Co, a broadening of the signal and larger Knight shifts were observed (320 ppm for CoMoP and 1830 ppm for Co_2P).

The catalytic activity of MoP/SiO_2, $CoMoP/SiO_2$, $NiMoP/SiO_2$, Co_2P/SiO_2, and WP/SiO_2 was measured in the HDN of *o*-methylaniline, and these phosphidic materials were compared to a classical HDN/HDS sulfidic $NiMo/Al_2O_3$ catalyst. MoP/SiO_2 and Co_2P/SiO_2 had a higher intrinsic activity than the sulfidic $NiMo/Al_2O_3$ material. The presence of Co and Ni together with Mo in the ternary phosphide compounds resulted in materials, the intrinsic activity of which was lower than that of the binary compounds MoP/SiO_2 and Co_2P/SiO_2. The loss of activity in the presence of H_2S, measured over all the materials, was attributed to the competitive adsorption of H_2S and the reactant molecules, while the increase in activity over MoP/SiO_2 after the removal of H_2S probably resulted from the creation of new MoS_2-type active sites from small Mo metal particles.

Acknowledgments

The authors thank Ms. K. Hametner and Prof. D. Günther for the elemental analyses (LA-ICP-MS) and Dr. L. Qu for the help with the HDN catalytic experiments.

References

[1] R. Prins, V.H.J. de Beer, G.A. Somorjai, Catal. Rev. Sci. Eng. 31 (1989) 1.
[2] H. Topsøe, B.S. Clausen, F.E. Massoth, Hydrotreating Catalysis, in: Science and Technology, Vol. 11, Springer, New York, 1996.
[3] T. Weber, R. Prins, R.A. van Santen (Eds.), Transition Metal Sulphides–Chemistry and Catalysis, Kluwer, Dordrecht, 1998.
[4] J.C. Schlatter, S.T. Oyama, J.E. Metcalfe, J.M. Lambert, Ind. Eng. Chem. Res. 27 (1988) 1648.
[5] H. Abe, T.K. Cheung, A.T. Bell, Catal. Lett. 21 (1993) 11.
[6] P.A. Aegerter, W.W.C. Quigley, G.J. Simpson, D.D. Ziegler, J.W. Logan, K.R. McCrea, S. Glazier, M.E. Bussell, J. Catal. 164 (1996) 109.
[7] S.T. Oyama (Ed.), The Chemistry of Transition Metal Carbides and Nitrides, Blackie Academic and Professional, London, 1996.
[8] W. Robinson, J.N.M. van Gestel, T.I. Koranyi, S. Eijsbouts, A.M. van der Kraan, J.A.R. van Veen, V.H.J. de Beer, J. Catal. 161 (1996) 539.
[9] W. Li, B. Dhandapani, S.T. Oyama, Chem. Lett. (1998) 207.
[10] C. Stinner, R. Prins, Th. Weber, J. Catal. 191 (2000) 438.
[11] C. Stinner, R. Prins, Th. Weber, J. Catal. 202 (2001) 187.
[12] P. Clark, W. Li, S.T. Oyama, J. Catal. 200 (2001) 140.
[13] S.T. Oyama, P. Clark, X. Wang, T. Shido, Y. Iwasawa, S. Hayashi, J.M. Ramallo-López, F.G. Requejo, J. Phys. Chem. B 106 (2002) 1913.
[14] C. Stinner, Z. Tang, M. Haouas, Th. Weber, R. Prins, J. Catal. 208 (2002) 456.
[15] S.T. Oyama, P. Clark, V.L.S. Teixeira da Silva, E.J. Lede, F.G. Requejo, J. Phys. Chem. B 105 (2001) 4961.
[16] N.P. Sweeny, C.S. Rohrer, O.W. Brown, J. Am. Chem. Soc. 80 (1958) 799.
[17] E.L. Muetterties, J.C. Sauer, J. Am. Chem. Soc. 96 (1974) 3410.
[18] F. Nozaki, R. Adachi, J. Catal. 40 (1975) 166.
[19] F. Nozaki, M. Tokumi, J. Catal. 79 (1983) 207.
[20] J.N. Heresnape, J.E. Morris, GB patent 701 217, 1953.
[21] J.N. Housam, R. Lester, GB patent 807 583, 1959.
[22] J.A.R. van Veen, H.A. Colijn, P. Hendriks, A.J. van Welsenes, Fuel Process. Technol. 35 (1993) 137.
[23] G. Nolze, W. Kraus, Powder Diffr. 13 (1998) 256.
[24] D. Günther, C.A. Heinrich, J. Anal. Atom. Spectrom. 14 (1999) 1363.
[25] H.P. Longerich, S.E. Jackson, D. Günther, J. Anal. Atom. Spectrom. 11 (1996) 899.
[26] R. Thomas, J.A. Moulijn, J. Mol. Catal. 8 (1980) 161.
[27] PDF 24-771.
[28] K. Eichele, R.E. Wasylishen, J. Phys. Chem. 98 (1994) 3108.
[29] G.C. Gunter, R. Craciun, M.S. Tam, J.E. Jackson, D.J. Miller, J. Catal. 164 (1996) 207.
[30] P. Clark, X. Wang, S.T. Oyama, J. Catal. 207 (2002) 256.

[31] V. Zuzaniuk, C. Stinner, R. Prins, Th. Weber, Stud. Surf. Sci. Catal. 143 (2002) 247.
[32] X. Wang, P. Clark, S.T. Oyama, J. Catal. 208 (2002) 321.
[33] W.E. Blumberg, Phys. Rev. 119 (1960) 79.
[34] S. Rundqvist, Acta Chem. Scand. 14 (1960) 1961.
[35] R. Guerin, M. Sergent, Acta Crystallogr. B 33 (1978) 2820.
[36] W.D. Knight, S. Kobayashi, in: D.M. Grant, R.K. Harris (Eds.), Encyclopedia of Nuclear Magnetic Resonance, Wiley, Chechester, 1996, p. 2672.
[37] S. Ohta, H. Onmayashiki, Phys. B 253 (1998) 193.
[38] S. Wada, T. Matsuo, S. Takata, I. Shirotani, C. Sekine, J. Phys. Soc. Jpn. 69 (2000) 3182.
[39] T.I. Korányi, Appl. Catal. A 239 (2003) 253.
[40] T. Shido, R. Prins, J. Phys. Chem. B 102 (1998) 8426.
[41] M. Jian, R. Prins, J. Catal. 179 (1998) 18.
[42] K.S. Lee, H. Abe, J.A. Reimer, A.T. Bell, J. Catal. 139 (1993) 34.
[43] F. Rota, R. Prins, J. Mol. Catal. A 162 (2000) 359.
[44] M. Jian, R. Prins, Catal. Today 30 (1996) 127.